VIP Anisotropy Very Important Paper

Deutsche Ausgabe: DOI: 10.1002/ange.201511309
Internationale Ausgabe: DOI: 10.1002/anie.201511309

Layered Black Phosphorus: Strongly Anisotropic Magnetic, Electronic, and Electron-Transfer Properties

Zdeněk Sofer, David Sedmidubský, Štěpán Huber, Jan Luxa, Daniel Bouša, Chris Boothroyd, and Martin Pumera**

Abstract: *Layered elemental materials, such as black phosphorus, exhibit unique properties originating from their highly anisotropic layered structure. The results presented herein demonstrate an anomalous anisotropy for the electrical, magnetic, and electrochemical properties of black phosphorus. It is shown that heterogeneous electron transfer from black phosphorus to outer- and inner-sphere molecular probes is highly anisotropic. The electron-transfer rates differ at the basal and edge planes. These unusual properties were interpreted by means of calculations, manifesting the metallic character of the edge planes as compared to the semiconducting properties of the basal plane. This indicates that black phosphorus belongs to a group of materials known as topological insulators. Consequently, these effects render the magnetic properties highly anisotropic, as both diamagnetic and paramagnetic behavior can be observed depending on the orientation in the magnetic field.*

Layered black phosphorus belongs to the class of layered materials, which have been attracting great attention over the last few years.[1] These materials have a huge application potential in modern technologies.[2] The structure of black phosphorus exhibits strong covalent bonds within the layer plane and weak van der Waals forces between individual layers. Layered materials, such as graphite, layered transition-metal dichalcogenides (TMDs), or black phosphorus, are currently at the forefront of research targeting numerous applications related to energy storage and conversion, electrochemical catalysis, and sensors.[3]

The anisotropy of layered materials, such as graphite and TMDs, does not only concern their inherent electronic and thermal transport properties, but it also dominates their heterogeneous electron-transfer characteristics, which are directly reflected by their electrochemical behavior.[4] This is related to the fast heterogeneous electron transfer proceeding predominantly on the layer edges or at defects within the layers in the case of graphite and TMDs. In general, the basal planes of layered materials exhibit only very weak electrochemical activity to inner-sphere molecular probes whereas the heterogeneous electron-transfer rates of the edge sites are much faster.

Given the importance of layered materials, such as graphite or TMD, in industrial applications, it is imperative to investigate the anisotropy of the properties of black phosphorus. Herein, we investigate the electrochemical, electronic, and magnetic properties of black phosphorus single crystals with edge- and basal-plane-oriented surfaces. Insight into the electrochemistry of black phosphorus is provided by experiments and ab initio calculations of the electronic structure, which manifest the distinct properties of the basal- and edge-plane surfaces compared to the bulk material. Our DFT calculations showed the metallic character of the edge-surface states, indicating behavior typical of a topological insulator, which has not been reported for black phosphorus ever before.[5] Magnetic measurements revealed an extreme anisotropy of the magnetic susceptibility; the edge-plane localization of magnetic moments led to a paramagnetic behavior of edge-plane-oriented material in contrast to a dominant diamagnetic response for the basal-plane orientation. The anisotropy of the heterogeneous electron-transfer properties even to outer-sphere probes as well as of the magnetic and transport properties is highly relevant not only for the whole electrochemical community, but generally from a material chemistry perspective. Our findings point to potential applications of black phosphorus for energy storage and generation.

High-quality black phosphorus crystals (see the Supporting Information, Figure S1) for electrode construction were prepared by vapor transport growth. The morphology of the crystals was further investigated by SEM and TEM. The SEM images are shown in Figure 1 A and Figure S2 and clearly manifest the layered structure of the black phosphorus crystal. No additional elements, such as oxygen, or other impurities were observed by energy-dispersive spectroscopy (EDS; Figure S2). TEM was performed together with selective area electron diffraction (SAED) and electron energy loss spectroscopy (EELS). TEM images together with the corresponding SAED and EEL spectra are shown in Figure 1 B and Figure 1 C, respectively. The SAED pattern taken from a single grain shows the high quality of the crystals. The

[*] Prof. Dr. M. Pumera
Division of Chemistry and Biological Chemistry
School of Physical and Mathematical Sciences
Nanyang Technological University
Singapore 637371 (Singapore)
E-mail: pumera@ntu.edu.sg
Prof. Dr. Z. Sofer, Prof. Dr. D. Sedmidubský, Dr. Š. Huber, J. Luxa, D. Bouša
Department of Inorganic Chemistry
University of Chemistry and Technology Prague
Technická 5, 16628 Prague 6 (Czech Republic)
E-mail: zdenek.sofer@vscht.cz
Dr. C. Boothroyd
Ernst Ruska-Centrum and Peter Grünberg Institute
Forschungszentrum Jülich
52425 Jülich (Germany)

Supporting information for this article is available on the WWW under http://dx.doi.org/10.1002/anie.201511309.

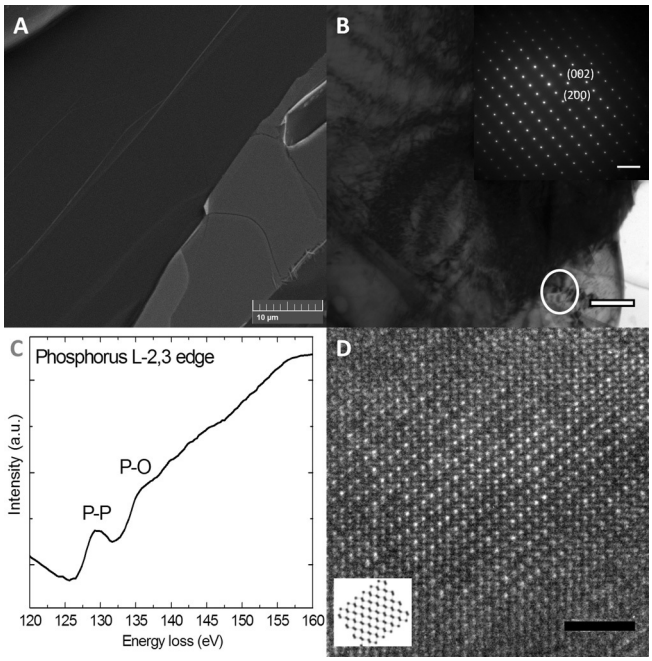

Figure 1. A) The surface of a black phosphorus crystal imaged by SEM. B) TEM image of black phosphorus crystals and the corresponding SAED pattern. Scale bars: 500 nm (TEM) and 5 nm^{-1} (SAED). The circle corresponds to the area used for the SAED pattern and EEL spectrum. C) EEL spectrum of a black phosphorus crystal. D) HRTEM image of a black phosphorus crystal. A structural model of black phosphorus with a similar orientation is shown in the left corner. Scale bar: 2 nm.

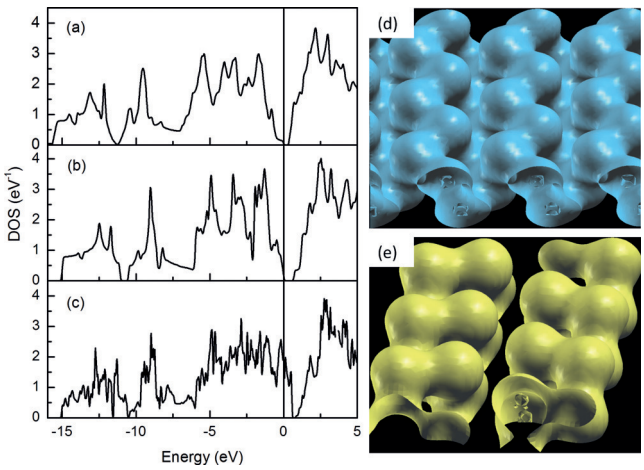

Figure 2. Density of states of black phosphorus with a) a bulk structure, b) as a monolayer, c) as a slab with the surface perpendicular to the layers. A 15 Å thick vacuum was introduced in (b) and (c) to separate the blocks. d, e) Valence electron density of a single layer (perpendicular to the (010) direction) of black phosphorus (d) and of a surface perpendicular to the (100) direction (e).

onset of the phosphorus absorption edge can be seen at 128 eV, and the edge shape is consistent with those observed by Favron et al.[8] A weak peak at 136 eV indicates some oxidation of the black phosphorus, which could have occurred during TEM sample preparation. The oxygen K-edge at 532 eV was also observed. This indicates that only negligible oxidation of the black phosphorus has occurred during the grinding step for TEM sample preparation. A corresponding HRTEM image of black phosphorus is shown in Figure 1 D.

The highly anisotropic properties of black phosphorus were also investigated by XRD, where preferential orientation along the (0*k*0) direction was observed. X-ray photoelectron spectroscopy (XPS) corroborated the high purity and negligible oxidation of the black phosphorus surface. Further characterization by XRD, FT-IR transmittance, and Raman spectroscopy of the basal- and edge-plane surfaces is shown and discussed in the Supporting Information (Figure S3).

Detailed DFT calculations of different black phosphorus surfaces were performed to understand the experimental data. The two-dimensional character of the phosphorus structure (space group *Cmca*), whose valence electron density is depicted in Figure 2 d, is manifested by a very small difference in the total energy, $+0.4\ kJ\,mol^{-1}$, between the single-layer and the bulk structure, as well as a negligible surface energy, $9\ mJ\,m^{-2}$ (referring to one side of a single layer). By contrast, a slab calculation with a surface perpendicular to the layers (Figure 2 e) differs by $+20.2\ kJ\,mol^{-1}$ and exhibits a surface energy of $194\ mJ\,m^{-2}$. Such an energetic surface is indeed highly receptive to the adsorption of various species and can thus exhibit an increased catalytic activity, which might be further accentuated by the orientation of lone pairs outwards from the surface (a feature also present on the standard (010) surface). This is in good correlation with the electrochemical investigation of edge-plane electrodes, where significant electrochemical activity was observed in comparison with the basal plane.

The calculated densities of states of both the bulk structure and a single monolayer (Figure 2 a and Figure 2 b) exhibit narrow band gaps with widths of 0.25 eV and 0.51 eV, respectively. These results slightly underestimate the band-gap energies (0.31–0.36 eV) observed experimentally for the bulk material,[6] which is a well known feature of canonical DFT functionals. To reproduce the experimental band gap properly, hybrid functionals with adjustable mixing parameters have to be applied.[6] The band-gap energy of a black phosphorus monolayer has not, to the best of our knowledge, been reported to date, but the discrepancy in DFT calculations can be explained in a similar manner as for the bulk form. Furthermore, we performed measurements of the bulk optical band gap, which was found to be 0.43 eV (Figure S3 B). This value is slightly higher than values reported previously.[6] As demonstrated in Figure S5, which shows the band structure of the monolayer, the band gap is direct and located at the *p*-point. Surprisingly, the slab structure with a surface perpendicular to the layers reveals a metallic character with a relatively high density of states at the Fermi level (see Figure 2 c). The states at the Fermi surface can be primarily identified with the atoms located on the surface with a slight extension to the second and third sheet below the surface.

For electrochemical applications, the work function of black phosphorus used as an electrode material is of pivotal importance. For this purpose, it is convenient to convert the work function from the reference vacuum level into the

potential relative to the SHE. When using this electrochemical scale, we obtained values of +0.21 V for the "bulk material" (a slab with a surface parallel to the layers separated by a 15 Å thick vacuum), 0.48 V for the monolayer, and 1.11 V for the slab with a metallic surface. The metallic conductivity and the trend in theoretical hydrogen overpotential obtained by ab initio calculations are in good agreement with various electrochemical measurements, such as the hydrogen evolution reaction, where a significantly lower overpotential was observed for the edge plane compared to the basal plane. Furthermore, the redox activity investigated by the two basic redox probes $[Fe(CN)_6]^{3-/4-}$ and $[Ru(NH_3)_6]^{2+/3+}$ exhibits significant differences between the basal plane and the edge plane. This can be explained by the metallic character of the black phosphorus edges as shown by the theoretical calculations. Such a topological dependence of the conductivity is typical for topological insulators such as bismuth and antimony telluride. These findings help to explain the strong anisotropy of the magnetic properties, which are discussed below.

Interestingly, the large anisotropy is also manifested by considerably different behavior when a magnetic field is applied perpendicular or parallel to the basal plane (see Figure 3 for magnetic susceptibility measurements). In both

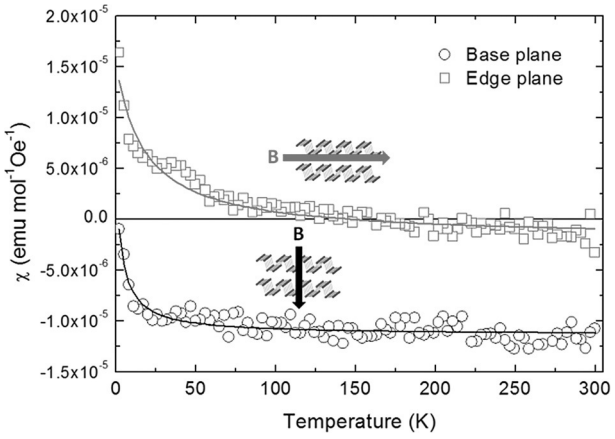

Figure 3. Magnetic susceptibility as a function of temperature measured for perpendicular (base plane, black) and parallel (edge plane, red) orientations with respect to the external field (1 kOe).

cases, an appreciable paramagnetic component is observed. As a Curie–Weiss fit yields a total spin value that is five times larger for the edge-plane orientation (corresponding to the concentration of unpaired spins, 1.2×10^{-3}), we can infer that the paramagnetic moments are localized on the edge planes and likely to be associated with the surface defects. Indeed, the obtained effective magnetic moment for the base-plane orientation is apparently suppressed by a lower demagnetizing factor (edges parallel to the field). The respective Weiss constants, −4 K and −18 K, determined for the base- and edge-plane orientations, respectively, point to weak antiferromagnetic correlations between the localized moments. More importantly, a strong anisotropy (one order in magnitude) comparable to that of graphite is observed for the diamagnetic component. For the edge-plane orientation, the diamagnetic susceptibility (considered as invariant with temperature), $\chi_{DM} = -1.9 \times 10^{-6}$ emu mol^{-1} Oe^{-1}, can be attributed to Langevin diamagnetism of phosphorus core electrons; however, the value obtained for the basal plane, $\chi_{DM} = -1.2 \times 10^{-5}$ emu mol^{-1} Oe^{-1}, has to be interpreted in terms of the Landau diamagnetism of itinerant charge carriers (induced by p-type doping), which, as for graphene, overwhelms the Pauli paramagnetic component. In fact, both contributions can compensate each other in the case of edge-plane orientation or can be negligible owing to a low concentration of charge carriers, which is also consistent with much higher resistivity.

To confirm the theoretical prediction obtained by ab initio calculations, we prepared basal-plane and edge-plane electrodes from black phosphorus. The morphology of the electrode surface was characterized by SEM and AFM (Figure S6). Resistivity measurements performed on a single crystal showed large anisotropy with an in-plane resistivity of 0.011 Ω cm, whereas the through-plane specific resistivity was only 180.2 Ω cm. The large anisotropy of the electrical resistivity projects a new view on the anisotropy of the electrochemical behavior of black phosphorus single crystals.

First, we investigated the inherent electrochemistry of black phosphorus electrodes with basal- and edge-plane orientations in 50 mmol PBS (pH 7.0). Significant differences were observed for these two electrode orientations. The edge-plane electrode exhibited a significantly narrower electrochemical window owing to the oxidation of phosphorus, which starts at +0.5 V (Figure 4 D). A slight increase in the current density can be observed for the basal-plane electrode as well; however, the current density is significantly lower.[9] This weak signal could originate from the oxidation of the few remaining edges on the basal-plane electrode, which was formed by mechanical cleaving of bulk phosphorus crystals. Such steps were also observed in a SEM image of the basal-plane electrode (Figure S6). It was possible to observe a weak reduction of the signal on the basal-plane electrode starting at about +0.25 V and reaching maxima at 0 V and −0.2 V for the first and second scan, respectively. This can be attributed to the presence of P^V on the electrode surface and its reduction (to P^{III} and P^I). A slight oxidation of the basal-plane electrode surface was observable in the AFM image of the basal-plane electrode surface (Figure S6).

The HET rate and the electron transfer mechanism were investigated with $[Fe(CN)_6]^{3-/4-}$ and $[Ru(NH_3)_6]^{3+/2+}$ redox probes. In both cases, we observed significant differences in the electrochemical activities of different phosphorus surfaces. Whereas in the case of $[Fe(CN)_6]^{3-/4-}$, no redox peak was observed for the basal plane, both oxidation and reduction were detected on the edge-plane electrode (Figure 4 A). The oxidation peak of $[Fe(CN)_6]^{4-}$ at 384 mV is clearly visible, whereas the reduction peak of $[Fe(CN)_6]^{3-}$ is superimposed with inherent electrochemical processes and shows a barely visible maximum at 197 mV. This corresponds to a peak-to-peak separation of 187 mV.

The oxidation of the outer-sphere probe $[Ru(NH_3)_6]^{2+}$ consists of waves at −43 mV and 136 mV at the edge plane of black phosphorus (Figure 4 B). The reduction wave of the

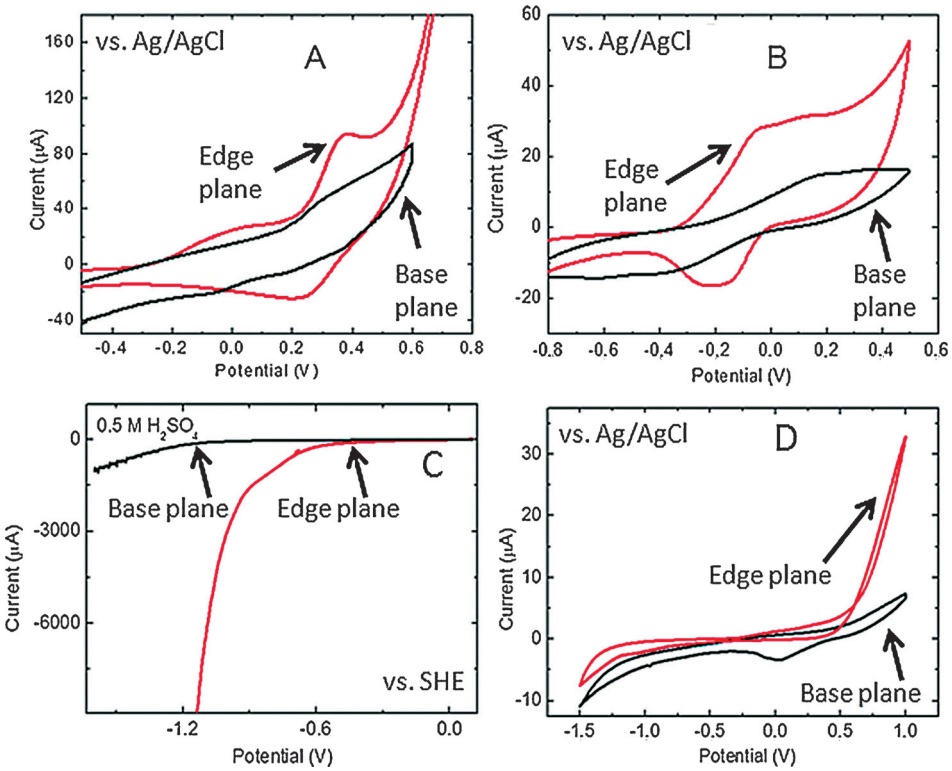

Figure 4. A) Cyclic voltammograms with $[Fe(CN)_6]^{3-/4-}$ as the redox probe for basal- and edge-plane black phosphorus electrodes. B) Cyclic voltammograms with $[Ru(NH_3)_6]^{2+/3+}$ as the redox probe for basal- and edge-plane phosphorus electrodes. Conditions for (A) and (B): 0.01 mol $[Fe(CN)^6]^{3-/4-}$ and $[Ru(NH_3)_6]^{2+/3+}$ in 0.05 M PBS, pH 7.0, scan rate: 100 mVs^{-1}, potential with respect to the saturated Ag/AgCl electrode. C) The hydrogen evolution reaction on basal- and edge-plane black phosphorus electrodes; $c(H_2SO_4) = 0.5$ mol, scan rate: 10 mVs^{-1}, potentials vs. RHE. D) The inherent electrochemistry of black phosphorus measured in phosphate buffer; $c = 0.05$ mol, pH 7.0, scan rate: 100 mVs^{-1}, potential vs. saturated Ag/AgCl electrode.

$[Ru(NH_3)_6]^{3+}$ redox pair has a maximum at −215 mV. These values correspond to a peak-to-peak separation of 172 mV. The redox activity of the ruthenium complex at the basal plane is poorly defined, with an oxidation peak at approximately 200 mV, a reduction peak at about −350 mV, and no other clear redox peaks. The electrochemical response of the $[Fe(CN)_6]^{3-/4-}$ redox probe for the basal- and edge-plane black phosphorus electrodes is similar to that of the ruthenium salt, where the edge planes are much more active ($\Delta E = 187$ mV) than the basal plane (see Figure 4B).

On the basis of previous results, we investigated the catalytic properties of basal- and edge-plane black phosphorus towards the hydrogen evolution reaction. The results of the hydrogen evolution reaction are shown in Figure 4C. Significant differences in the catalytic activities were observed, while reduction of the edge-plane phosphorus started at −0.55 V. Compared to edge-plane phosphorus, basal-plane phosphorus exhibits a very poor catalytic activity towards hydrogen evolution, and this starts at a potential as high as −1.13 V. The potential recalculated against the standard hydrogen electrode is −0.35 V for edge-plane and −0.93 V for basal-plane black phosphorus. A similar trend was obtained from ab initio calculations, where a metallic character was predicted for the edge-plane surface of black phosphorus.

Finally, we investigated the oxidation of biologically important compounds, such as ascorbic acid and dopamine, at the basal and edge plane of black phosphorus (Figure 5). A significantly higher sensitivity of the edge plane compared to the basal plane was observed for all investigated analytes. With ascorbic acid, the oxidation peak obtained with the edge-plane electrode starts at 35 mV and reaches a maximum at about 500 mV (Figure 5A). A similar trend was observed for the basal-plane electrode; however, the current was about one order of magnitude lower. For dopamine, the oxidation starts at +10 mV and reaches a maximum at about 440 mV (Figure 5B). As in the ascorbic acid electrochemistry, the current for the basal-plane electrode was about one order of magnitude lower.

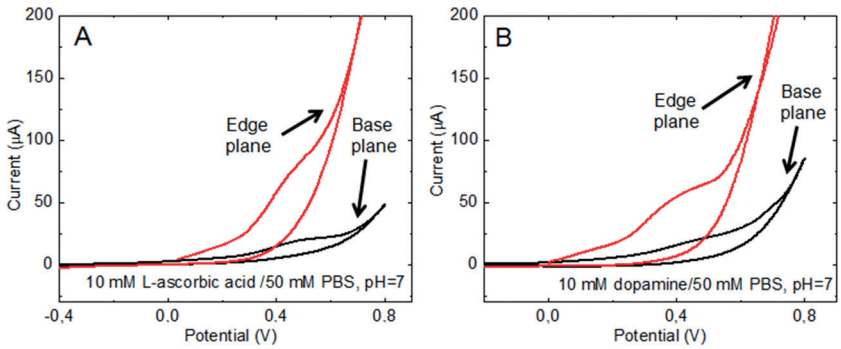

Figure 5. The activity of black phosphorus towards biosensing applications using ascorbic acid (Figure 5A) and dopamine (Figure 5B) as analytes and basal-plane and edge-plane black phosphorus electrodes. $c(PBS) = 0.05$ mol, $c(analyte) = 0.01$ mol, scan rate: 100 mVs^{-1}.

In summary, the anisotropy of the electrical, magnetic, and electrochemical properties of black phosphorus has been investigated in detail. The results of electrochemical and magnetic measurements are in good agreement with ab initio calculations for various crystallographic orientations of black

phosphorus. The significantly higher electrochemical activity of the black phosphorus edges compared to the basal plane can be explained by the metallic character of the edges, as determined by the calculations. Our results show that black phosphorus is a topological insulator with considerable differences in the electronic structure and electric properties of its different crystallographic surfaces. This is also associated with an extreme anisotropy of the magnetic properties; diamagnetic behavior was observed with a magnetic field perpendicular to the basal plane whereas a paramagnetic signal was detected for a crystal with the edge planes oriented perpendicularly to the magnetic field. Our findings are of particular significance for the application of black phosphorus not only in electrocatalysis, but also in electronic devices.

Experimental Section

The synthesis of black phosphorus crystals was based on a procedure reported in the literature[7] using an Au/Sn alloy-like solvent for red phosphorus and SnI_4 as a mineralizing agent in a sealed ampoule. 500 mg of the Au/Sn alloy were prepared by melting stoichiometric amounts of tin and gold under high vacuum directly in the ampoule used for the synthesis. 720 mg of red phosphorus and 15 mg of SnI_4 were added to a quartz ampoule, which was subsequently sealed by using an oxygen/hydrogen torch. The ampoule was placed in a muffle furnace and heated to 400 °C for 1 h. After leaving it at 400 °C for 2 h, the ampoule was heated to 600 °C for 24 h. The furnace was cooled to room temperature overnight. Crystals of black phosphorus shaped into plates with sizes of up to 15×4 mm were formed. For details, see the Supporting Information.

Cyclic voltammetry measurements were carried out with an Autolab PGSTAT 204. X-ray powder diffraction data were collected with a Bruker D8 Discoverer θ-θ diffractometer. An inVia Renishaw Raman microscope was used for Raman spectroscopy in backscattering geometry (laser: 532 nm, 5 mW). High-resolution XPS was performed on an ESCAProbeP spectrometer equipped with a monochromatic aluminum X-ray radiation source (1486.7 eV). The transmittance was measured using the FT-IR spectrometer iS50R (Thermo Scientific, USA). The AFM measurements were carried out on an Ntegra Spectra from NT-MDT. HRTEM images were taken using a FEI Titan "Holo" G2 60-300 microscope. The morphology of black phosphorus was investigated by SEM with an FEG electron source (Tescan Lyra dual beam microscope). The magnetic properties were measured with the Physical Property Measurement System (PPMS) EverCool-II (Quantum Design, USA) using the VSM option. More details for all characterization methods are given in the Supporting Information.

Acknowledgements

This project was supported by the Czech Science Foundation (GACR No. 15-09001S) and Specific University Research (MSMT No. 20/2015). M.P. was supported by a Tier 1 grant (0/13) from the Ministry of Education, Singapore. The research leading to these results received funding from the European Union Seventh Framework Programme under Grant Agreement 312483-ESTEEM2 (Integrated Infrastructure Initiative-I3).

Keywords: anisotropy · black phosphorus · electrochemical impedance spectroscopy · electronic structure · magnetic properties

How to cite: *Angew. Chem. Int. Ed.* **2016**, *55*, 3382–3386
Angew. Chem. **2016**, *128*, 3443–3447

[1] a) F. Xia, H. Wang, Y. Jia, *Nat. Commun.* **2014**, *5*, 4458; b) L. Li, Y. Yu, G. J. Ye, Q. Ge, X. Ou, H. Wu, D. Feng, X. H. Chen, Y. Zhang, *Nat. Nanotechnol.* **2014**, *9*, 372–377; c) S. P. Koenig, R. A. Doganov, H. Schmidt, A. C. Neto, B. Oezyilmaz, *Appl. Phys. Lett.* **2014**, *104*, 103106.

[2] a) M. Engel, M. Steiner, P. Avouris, *Nano Lett.* **2014**, *14*, 6414–6417; b) M. Buscema, D. J. Groenendijk, S. I. Blanter, G. A. Steele, H. S. van der Zant, A. Castellanos-Gomez, *Nano Lett.* **2014**, *14*, 3347–3352; c) Y. Du, H. Liu, Y. Deng, P. D. Ye, *ACS Nano* **2014**, *8*, 10035–10042; d) H. Wang, X. Wang, F. Xia, L. Wang, H. Jiang, Q. Xia, M. L. Chin, M. Dubey, S.-j. Han, *Nano Lett.* **2014**, *14*, 6424–6429.

[3] a) C. M. Park, H. J. Sohn, *Adv. Mater.* **2007**, *19*, 2465–2468; b) M. Buscema, D. J. Groenendijk, G. A. Steele, H. S. van der Zant, A. Castellanos-Gomez, *Nat. Commun.* **2014**, *5*, 4651; c) H. Liu, Y. Du, Y. Deng, D. Y. Peide, *Chem. Soc. Rev.* **2015**, *44*, 2732–2743; d) M. Pumera, A. H. Loo, *TrAC Trends Anal. Chem.* **2014**, *61*, 49–53; e) A. Y. S. Eng, A. Ambrosi, Z. Sofer, P. Šimek, M. Pumera, *ACS Nano* **2014**, *8*, 12185–12198; f) M. Pumera, Z. Sofer, A. Ambrosi, *J. Mater. Chem. A* **2014**, *2*, 8981–8987; g) M. Giovanni, H. L. Poh, A. Ambrosi, G. Zhao, Z. Sofer, F. Šaněk, B. Khezri, R. D. Webster, M. Pumera, *Nanoscale* **2012**, *4*, 5002–5008; h) A. N. Abbas, B. Liu, L. Chen, Y. Ma, S. Cong, N. Aroonyadet, M. Köpf, T. Nilges, C. Zhou, *ACS Nano* **2015**, *9*, 5618–5624; i) Q. Chen, L. Zhang, G. Chen, *Anal. Chem.* **2012**, *84*, 171–178.

[4] a) S. M. Tan, A. Ambrosi, Z. Sofer, Š. Huber, D. Sedmidubský, M. Pumera, *Chem. Eur. J.* **2015**, *21*, 7170–7178; b) T. J. Davies, M. E. Hyde, R. G. Compton, *Angew. Chem. Int. Ed.* **2005**, *44*, 5121–5126; *Angew. Chem.* **2005**, *117*, 5251–5256; c) C. C. M. Neumann, C. Batchelor-McAuley, C. Downing, R. G. Compton, *Chem. Eur. J.* **2011**, *17*, 7320–7326; d) R. L. McCreery, *Chem. Rev.* **2008**, *108*, 2646–2687; e) A. Ambrosi, T. Sasaki, M. Pumera, *Chem. Asian J.* **2010**, *5*, 266.

[5] C.-G. Andres, V. Leonardo, P. Elsa, O. I. Joshua, K. L. Narasimha-Acharya, I. B. Sofya, J. G. Dirk, B. Michele, A. S. Gary, J. V. Alvarez, W. Z. Henny, J. J. Palacios, S. J. v. d. Z. Herre, *2D Materials* **2014**, *1*, 025001.

[6] H. Liu, A. T. Neal, Z. Zhu, Z. Luo, X. Xu, D. Tománek, P. D. Ye, *ACS Nano* **2014**, *8*, 4033–4041.

[7] L. Wang, Z. Sofer, M. Pumera, *ChemElectroChem* **2015**, *2*, 324–327.

[8] A. Favron, E. Gaufrès, F. Fossard, L. Lèvesque, A. Phaneuf-L'Heureux, N. Tang, A. Loiseau, R. Leonelli, S. Francoeur, R. Martel, *arXiv* **2014**, 1408.

[9] S. Sugai, I. Shirotani, *Solid State Commun.* **1985**, *53*, 753–755.

Received: December 6, 2015
Published online: January 28, 2016

